Comparison of the Thermodynamic Stabilities and Solution Conformations of DNA·RNA Hybrids Containing Purine-Rich and Pyrimidine-Rich Strands with DNA and RNA Duplexes†

Jeffrey I. Gyi,‡ Graeme L. Conn,§ Andrew N. Lane,*,‡ and Tom Brown§

Division of Molecular Structure, National Institute for Medical Research, The Ridgeway, Mill Hill, London NW7 1AA, U.K., and Department of Chemistry, University of Southampton, Southampton SO17 1BJ, U.K.

Received April 19, 1996; Revised Manuscript Received July 12, 1996⊗

ABSTRACT: The conformations and thermodynamic stabilities of duplexes containing purine-rich (GAAGAGAAGC) and pyrimidine-rich (GCTTCTCTTC or GCUUCUCUUC) DNA and RNA strands have been measured by UV melting, electrophoresis, circular dichroism, and NMR spectroscopy. The free energies of stabilization ($-\Delta G$) were in the order rR·rY > rR·dY > dR·dY > dR·rY. The two DNA·RNA hybrid duplexes showed conformational properties intermediate between those of DNA·DNA and RNA·RNA duplexes and also different from one another. Differences between ^{1}H chemical shifts of the DNA strands in the two hybrid duplexes and those of the DNA duplex were larger than analogous shift differences for the RNA protons, and the differences were larger for the purine than the pyrimidines in the DNA strands. Detailed analysis of the nucleotide conformations using both NOE and scalar coupling data showed that the sugar conformations of the ribonucleotides are all near C3′-endo. The deoxyribonucleotides were in the "S" domain, i.e., near C2′-endo in the DNA duplex, and C1′-exo to C2′-endo in the two hybrids. However, the deoxyriboses in the two hybrids appear more flexible than in the DNA duplex, with the fraction in the "N" (C3′-endo) state increasing in the order dR·dY < dR·rY < rR·dY. Globally, the pure DNA duplex was B-form and the pure RNA duplex A form. The two DNA·RNA hybrids were neither A nor B, but closer globally to the A than the B form. The less stable dR·rY duplex has a significantly different conformation from rR·dY both at the local nucleotide level and globally.

Hybrid duplexes comprising a DNA and an RNA strand occur in several important biological processes. They are intermediates in transcription (Hanson & McClure, 1980), in DNA replication (Adams et al., 1986), and in the synthesis of retroviral cDNA by reverse transcription (Varmus, 1988). They are substrates for the ubiquitous RNAseH which catalyzes the hydrolysis of RNA only when it is present in an RNA·DNA hybrid duplex and not when it is part of an RNA·RNA duplex (Stein & Hausen, 1969). RNAse H shows little if any sequence specificity (Oda et al., 1993), and it has been recently suggested that the enzyme recognizes a difference in conformation between RNA·DNA hybrid and RNA·RNA duplexes (Fedoroff et al., 1993; Lane et al., 1993).

DNA·RNA hybrids are also exploited in antisense technology (Stein & Cheng, 1993). However, because the target RNA is likely to be present at low concentration, optimal thermodynamic stability of the proposed hybrids is desirable. It has been reported, however, that the thermodynamic stability of hybrid duplexes in which the DNA strand consists of purines and the RNA strand consists of pyrimidines (dR·rY) is much less than the corresponding duplex containing a purine RNA strand and a pyrimidine DNA strand (rR·dY) (Ratmeyer et al., 1994; Hung et al., 1994; Wang & Kool, 1995; Lesnik & Freier, 1995). These studies demonstrated that the thermodynamic stabilities of the four kinds of duplex are dependent on the base composition. Further, the measured free energies of stabilization agree reasonably well with nearest neighbor calculations (Breslauer et al., 1986, Freier et al., 1986, Sugimoto et al., 1995). The origin of the differences was recently rationalized in terms of the chemical differences arising from the 5-Me of T in the DNA and the 2′-OH of the riboses in RNA (Wang & Kool, 1995). The influence of different conformations was not addressed in this study. It has been shown that the solution conformation of DNA·RNA hybrids of mixed sequence is neither the A-form of typical of duplex RNA nor the B form typical of duplex DNA, though the overall conformation is closer to the A form than to the B form (Fedoroff et al., 1993; Lane et al., 1993; Gonzalez et al., 1995). Further, both electrophoretic properties and circular dichroism indicated that the rR·dY and dR·rY hybrids have different global conformations; rR·dY is more like RNA (i.e., A form) whereas dR·rY is intermediate between the DNA and RNA duplexes (Ratmeyer et al., 1994; Hung et al., 1994). Recent work has suggested that there may be a continuum of structures between the A and B forms depending on the composition of the strands (Lesnik & Freier, 1995).

To assess the conformational contribution to the thermodynamic stability of DNA·RNA hybrids of different base composition, it is necessary to determine their structures in solution, and compare them with their "parent" homodu-

† This work was supported by the Medical Research Council of the U.K. and a Royal Society of Edinburgh Caledonian Research Fellowship to G.C.

* Address correspondence to this author at Division of Molecular Structure, National Institute for Medical Research, The Ridgeway, Mill Hill, London NW7 1AA, U.K. Telephone: 0181 959 3666, ext. 2052. Fax: 0181 906 4477. E-mail: a-lane@nimr.mrc.ac.uk.

‡ National Institute for Medical Research.

§ University of Southampton.

⊗ Abstract published in *Advance ACS Abstracts,* September 1, 1996.

S0006-2960(96)00948-8 CCC: $12.00

plexes. To this end, we have made four decamer duplexes containing a purine-rich and a pyrimidine-rich strand, and we have compared their properties using a combination of thermodynamics, electrophoresis, circular dichroism, and ^{1}H and ^{31}P NMR spectroscopy. In this article we report the differences in both local and global conformational features and dynamic aspects of the deoxynucleotide strands.

MATERIALS AND METHODS

Materials. d(GAAGAGAAGC) and d(GCTTCTCTTC) were synthesized and purified using standard methods as previously described (Brown & Brown, 1991, 1992). The analogous RNA strands r(GAAGAGAAGC) and r(GCUUCUCUUC) were synthesized on an ABI 349A automated synthesizer on a 1 μmol scale using 2′-*O*-*tert*-butylsilyl protected ribonucleotide phosphoramidites and derivatized polystyrene supports (Applied Biosystems). The 2′-OH protecting group was removed with triethylammonium fluoride in NMP for 30−60 min at 65 °C (Wincott et al., 1995). Oligonucleotides were cleaved from the solid support and the bases deprotected by treatment with concentrated ammonia/ethanol (3:1) at 55 °C for 4 h. The crude products were purified by reverse-phase HPLC (Brownlee Aquapore, 250 by 10 mm) using a gradient of 0−20% acetonitrile in 0.1 M ammonium acetate. Pooled fractions were desalted on Sephadex G10 and lyophilized. For brevity, we refer to these strands as dR10 and dY10 for the predominantly purine and pyrimidine DNA strands, respectively, and analogously rR10 and rY10 for the ribonucleotide strands.

Duplexes were formed by mixing equimolar concentrations of the appropriate strands as determined from their absorption coefficients. The duplexes were annealed, cooled on ice, and dialyzed at 4 °C against 10 mM sodium phosphate and 100 mM KCl, pH 7.0, using a 3.5 kDa cutoff membrane (Spectrapor), lyophilized, and redissolved in 0.6 mL of D_2O or 90% H_2O/10% D_2O for NMR analysis.

Methods. Melting temperatures, T_m, were determined as a function of concentration (range 70−100-fold) for each of the four possible duplexes on a Perkin-Elmer Lambda 2 UV/vis spectrophotometer using the PECSS2 software as previously described (Ebel et al., 1994). Unless otherwise stated, the melting curves were recorded in 10 mM sodium phosphate and 0.1 M NaCl, pH 7.0. Oligonucleotide concentrations were calculated from the absorbance and the measured absorption coefficients. Thermodynamic parameters were derived according to

$$1/T_m = (R/\Delta H)\ln(C_t/4) + \Delta S/\Delta H \quad (1)$$

where C_t is the concentration of stands, R is the gas constant, ΔH is the enthalpy, and ΔS is the entropy of melting. The standard state was taken to be at 1 μM strands and 25 °C.

UV spectra were recorded on a Hitachi U_3210 spectrophotometer equipped with thermostated cuvette holders. Absorption coefficients for the duplexes were determined by recording a spectrum under standard conditions in 0.05 M sodium acetate and 10 mM magnesium acetate, pH 5, followed by digestion with nuclease P1 (Pharmacia, Sweden). After the reaction was complete as monitored by the increase in the absorbance at 260 nm, the spectrum was recorded again. The concentration was determined from the known absorption coefficients of the mononucleotides (Fasman, 1975) and the composition. This was then used to calculate the absorption coefficient of the undigested sample. CD[1] spectra were recorded in 0.5 M KCl at 15 °C on a Jasco spectropolarimeter as previously described (Lane et al., 1993).

Comparative electrophoresis was carried out on minigels using 20% acrylamide and Tris borate−EDTA buffer. The gels were typically run at 150 V for 60−90 min at 4 °C, stained with ethidium bromide, and visualized using its fluorescence.

^{1}H NMR spectra were recorded at 11.75 and 14.1 T on Varian UnityPlus and Unity spectrometers, respectively. Spectra in H_2O were recorded at 10 °C using the Watergate method (Piotto et al., 1992) and at 30 and 35 °C in D_2O. Phase-sensitive two-dimensional NMR spectra were recorded using the method of States et al. (1982). Acquisition times were typically 0.4−0.5 s in t_2 and 0.05−0.06 s in t_1. TOCSY spectra were recorded using MLEV-17 for isotropic mixing (Bax & Davis, 1985) with mixing times of ca. 50 ms and a spin-lock field strength of 9 kHz. Data tables were zero-filled once in t_2 and twice in t_1 before Fourier transformation. Spectra were referenced to internal 2,2-dimethylsilapentane-5-sulfonate. Effective rotational correlation times were determined using time-dependent one-dimensional NOEs as previously described (Lane et al., 1986; Birchall & Lane, 1990).

^{31}P NMR spectra were recorded at 25 °C at 9.4 T on a Bruker AM400 spectrometer. The spectra were referenced to external methylene diphosphonate at 0 ppm. The acquisition time was 1.3 s, and a relaxation delay of 2 s was used. The spectra were processed using a Lorentz−Gauss function.

Relaxation rate constants R_1 and R_2 were measured as previously described (Forster & Lane, 1990). The heteronuclear NOE was measured using the gated decoupler experiment with a recycle time of $5T_1$. The rotational correlation time and CSA were estimated from the relaxation data by searching through values and finding the minimum of the target function:

$$\text{error} = |(R_1(\text{obs}) - R_1(\text{calc}))/R_1(\text{obs})| + (R_2(\text{obs}) - R_2(\text{calc}))/R_2\text{obs}| + (\text{NOE(obs)} - \text{NOE(calc)})/\text{NOEobs}| \quad (2)$$

where

$$R_1(\text{calc}) = 133.33\kappa^2{\omega_p}^2 J(\omega_p)10^{-6} + \sum 9.1/r^6[J(\Delta\omega) + 3J(\omega_p) + 6J(\sum\omega)] \quad (3)$$

$$R_2(\text{calc}) = 22.22\kappa^2{\omega_p}^2[4J(0) + 3J(\omega_p)]10^{-6} + \sum 4.5/r^6[4J(0) + J(\Delta\omega) + 3J(\omega_p) + 3J(\omega_p) + 6J(\sum\omega)] \quad (4)$$

$$\text{NOE} = 1 + 2.5[6J(\sum\omega) - J(\Delta\omega)]/R_1 \quad (5)$$

κ is the effective CSA, which is the product of the chemical shift anisotropy and the asymmetry parameter (Lane, 1994).

As the observed NOE was small, the values of R_1 and R_2 are dominated by the CSA term, so an initial estimate of the correlation time can be estimated from the ratio of R_2/R_1 (Williamson & Boxer, 1989).

[1] Abbreviations: DQF-COSY, double quantum filtered correlation spectroscopy; NOESY, nuclear Overhauser spectroscopy; TOCSY, total correlation spectroscopy; CSA, chemical shift anisotropy; CD, circular dichroism.

$$\tau = (1/2\omega_p)[6R_2/R_1 - 7]^{0.5} \quad (6)$$

An initial estimate of κ was obtained from the difference function $R_2 - 0.5R_1$ using the initial value of τ

$$R_2 - 0.5R_1 = 88.88\kappa^2\omega_p{}^2\tau 10^{-6} + \sum 4.5/r^6[4J(0) + 6J(\sum\omega)] \quad (7)$$

An initial value for r was taken as 2.1 Å (Forster & Lane, 1990), which is based on field-dependent measurements of the ^{31}P relaxation times and calculations on B and A form structures. The search was then conducted for values of κ and τ in the neighborhood of these initial values, for different values of r. As the dipolar term is small compared with the CSA term, the result is not very sensitive to r. The search gives a set of solutions that are compatible with the experimental results within experimental error and therefore provides an estimate of the variance of each fitted parameter.

Conformational Analysis. Sums of coupling constants were determined from the NOESY recorded with a long mixing time (250 ms) and DQF-COSY spectra. H1′−H4′ distances were estimated from cross-sections through H1′ of NOESY spectra. The ratio, R, of the cross-peak areas in cross-section of H1′−H4′ to H1′−H2″ is equal to the ratio of the cross-peak volume as H1′ is the common diagonal peak. This NOE is not significantly distorted by spin diffusion, and because $r_{1'2''}$ is essentially independent of sugar conformation ($r_{1'2''} = 2.35 \pm 0.05$ Å), $r_{1'4'}$ can be calculated from R as

$$r_{1'4'} = 2.35R^{-1/6} \quad (8)$$

Because H2″ relaxes faster than H4′, R is overestimated. This is compensated for by making measurements from NOESY spectra recorded at different mixing times and extrapolating back to zero mixing time.

Distances and coupling constants were simultaneously evaluated using a grid-search method assuming a two-state equilibrium between N and S sugar puckers as previously described (Conte et al., 1996). In these searches, the pseudorotation phase angle was held constant at 9°, and a systematic search was conducted over a range of the pseudorotation phase angle for the S state (P_s) and the fraction of the S state, f_s. The search was repeated for different values of the pucker amplitude ϕ_m between 30° and 42°, assuming that the amplitude is the same for both the N and S states. The combination of the coupling constants and these distances leads a better determination of the sugar conformations than either set of data individually (Conte et al., 1996).

Glycosidic torsion angles were determined by the combined grid-search and nonlinear regression to NOE build-up curves with the program NUCFIT (Lane, 1990), which accounts for spin diffusion, multiple sugar conformations, and the effects of incomplete longitudinal relaxation (Lane & Fulcher, 1995).

Distances between protons in sequential nucleotides, H2′-(i)−H8/H6(i+1) in the RNA strands and H2″(i)−H8/H6-(i+1) in the DNA strands, were calculated from NOESY cross-peak volumes normalized to those of the cytosine or uridine H6−H5 cross-peaks. These distances are diagnostic of A- and B-like helices. Volumes were calculated using Felix 95.0 (Biosym) either by direct volume integration or by fitting Gaussian functions to cross-sections in both dimensions through cross-peaks for overlapping peaks. For isolated peaks, these two methods agreed within 20%. Normalized volumes from spectra recorded at different mixing times (typically 50, 100, and 250 ms) were extrapolated linearly back to zero mixing time, and the distance was calculated assuming that r(H6−H5) = 2.45 Å. Simulations showed that, for the correlation times measured for these decamers, the linear extrapolation from 100 ms provides a reasonably precise estimate of the normalized volume at zero mixing time.

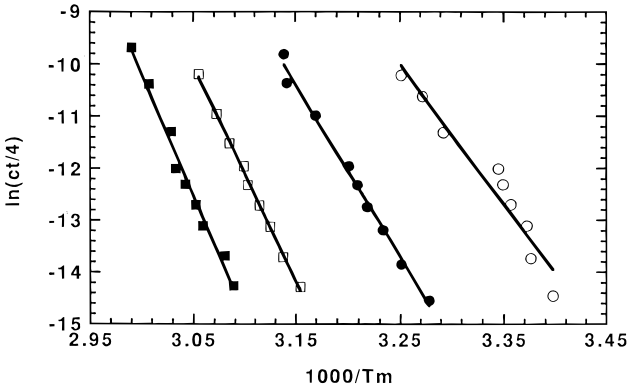

FIGURE 1: Dependence of melting temperatures on concentration. Melting temperatures for the four duplexes were measured as described in Materials and Methods. (●) dR10·dY10, (□) rR10·dY10, (○) dR10·rY10, (■) rR10·rY10.

RESULTS

Thermodynamic Stability. The thermodynamic stability of all four duplexes has been determined from the concentration dependence of the melting temperatures determined optically as described in Materials and Methods. Monophasic melting curves were obtained, and the dependence of the T_ms on concentration of strands (Figure 1) demonstrated the involvement of at least two strands in the observed transitions. The sequences of the oligonucleotides raise the possibility of triplex formation. However, at higher concentrations of nucleotides and comparable buffer conditions, the NMR spectra recorded at temperatures between 10 and 40 °C showed no evidence of triple helices (see below), which have characteristic spectral properties (Feigon et al., 1995). It is therefore unlikely that triple helices would form at the lower concentrations used in the optical studies. Furthermore, the kinds of intermolecular triple helices that might form would be expected to be very unstable in the absence of magnesium (Pilch et al., 1990), especially at neutral pH where the cytosines in the Hoogsteen strands of the parallel RY·Y triplex (with overhanging G on the third strand) would be unprotonated. The electrophoresis experiments (see below) showed no evidence of mixtures of duplexes and triple helices. The UV-melting curves showed no evidence of low-temperature transitions. Additional control experiments carried out with excess of one or the other strand at different pH values, in the absence or presence of magnesium and monitored at both 260 and 280 nm, failed to detect any triplex formation. We conclude that the transitions measured optically correspond primarily to melting of duplexes into single strands, and they have been analyzed accordingly. The thermodynamic parameters are collected in Table 1. The data have been obtained also at

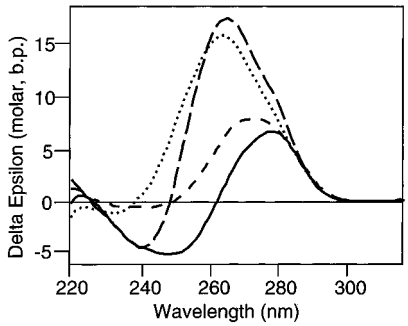

FIGURE 2: CD spectra of the four duplexes. Spectra were recorded at 15 °C as described in Materials and Methods. (—) dR·dY; (—·—) dR·rY; (—) rR·dY; (···) rR·rY.

Table 1: Thermodynamic Stability of the Four Decamer Duplexes[a]

duplex	$\Delta G(298)$ (kJ mol^{-1})	ΔH (kJ mol^{-1})	ΔS (kJ mol^{-1}/K)	T_m (1 μM) (K)	T_m (1 mM) (K)
dR10·dY10	−42.9	−290	−0.829	305	325
dR10·rY10	−31.8	−238	−0.693	291	313
rR10·dY10	−55.8	−343	−0.963	315	333
rR10·rY10	−66.9	−394	−1.098	322	338

[a] Thermodynamic parameters were determined from the concentration dependence of the T_m measured from UV melting curves as described in Materials and Methods. The T_m at 1 mM was calculated from the T_m measured at 1 μM and ΔH using eq 1 in the text.

different ionic strengths, from 0.1 to 1 M in salt at a fixed concentration of nucleotide. The slope of the T_m versus log [Na^+] was between 9 and 10, which is similar to the value reported by Ratmeyer et al. (1994) when the number of base pairs is taken into account. As expected, and consistent with other work (Hall & McLaughlin, 1991; Ratmeyer et al., 1994; Lesnik & Freier, 1995; Sugimoto et al., 1995; Wang & Kool, 1995), the RNA duplex is the most stable under all conditions. The order of stability based either on $\Delta G(298)$ or T_m is rR10·rY10 > rR10·dY10 > dR10·dY10 > dR10·rY10. Interestingly, the stabilities also follow the ΔH term, with the least stable dR10·rY10 duplex showing a low enthalpy, consistent with the poorest base-stacking.

Optical Spectroscopy. The absorption spectra of the four duplexes were similar, with λ_{max} between 257 and 258 nm, and the hyperchromicity for decomposing the duplexes into the component mononucleotides varied between 0.4 for the RNA duplex and the rR10·dY10 hybrid to 0.49 for the DNA duplex and dR10·rY10 hybrid.

The near-UV CD spectra of all four duplexes were recorded at a concentration of 40 μM duplex in 0.5 M KCl at 15 °C (Figure 2), where the oligonucleotides are >95% duplex (Table 1). The RNA duplex showed a typical nonconservative CD spectrum, with an intense positive peak at 264 nm and a weak negative peak at 232 nm. The DNA showed a typical conservative CD spectrum with a positive peak at 281 nm and a negative peak at 249 nm. The intensity in the spectrum of the RNA duplex was approximately 2.5-fold higher than that in the DNA spectrum (Figure 2). These spectral properties are typical of A- and B-like helices, respectively (Ivanov et al., 1974). The spectra of the two hybrids were intermediate between these two extremes, though in both cases the spectra were nonconservative, with features more A-like than B-like.

These results are comparable to those reported by Ratmeyer et al. (1994) for dodecamers consisting of alternating GA·CT base pairs. In all four duplexes studied here, the purine strands have identical base compositions, whereas in the pyrimidine strands there is the difference between U and T in the deoxy- or ribonucleotides. It is possible that different transition moments for T and U could produce significantly different spectra. However, in polymeric RNA of mixed sequence, the spectral properties are very similar to those of the RNA duplex reported here (Ivanov et al., 1974).

Table 2: Hydrodynamic Properties of the Four Decamer Duplexes[a]

duplex	μ_{rel}	τ_{cyt} (ns)	τ_p (ns)	CSA (ppm)
dR10·dY10	1.0	3.2 ± 0.3	3.6 ± 0.3	147 ± 7
dR10·rY10	0.92	nd	nd	nd
rR10·dY10	0.84	nd	2.95 ± 0.24	141 ± 7
rR10·rY10	0.77	2.9 ± 0.2	3.2 ± 0.2	154 ± 5

[a] μ_{rel} is the relative electrophoretic mobility on 20% acrylamide gels at 4 °C. τ_{cyt} and τ_p are effective correlation times at 30 °C determined by cross-relaxation between the H6 and H5 of cytosine and ^{31}P NMR relaxation, respectively. CSA is the effective chemical shift anisotropy as defined in the text, averaged over all phosphodiesters in each duplex. nd, not determined.

Electrophoresis. All duplexes have identical compositions and sequences (apart from the U for T substitutions in the RNA strands) and should have identical charges. Differences in electrophoretic or hydrodynamic properties therefore should arise primarily from differences in hydrodynamic volume (or shape). This could be due to gross differences in shape (such as B and A form), large differences in hydration or counterion condensation (which would depend on overall conformation), or differential interaction with the gel matrix. We have measured the electrophoretic mobility as summarized in Table 2. The order of mobility is dR10·dY10 > dR10·rY10 > rR10·dY10 > rR10·rY10, which agrees with the order reported by Ratmeyer et al. (1994). The clear ordering of mobilities suggests that the global shapes of the two hybrids are not identical, but that rR10·dY10 is more akin to the RNA duplex, and dR10·rY10 is more similar to the DNA duplex.

NMR Spectroscopy. The thermodynamic, spectroscopic, and hydrodynamic data confirm that there are differences between the two DNA·RNA hybrids. To probe the conformational differences in greater detail, we have applied ^{1}H NMR spectroscopy. The protons of the four duplexes have been assigned using NOESY, DQF-COSY, and TOCSY.

d(GAAGAGAAGC)·d(GCTTCTCTTC). Figure 3 shows the low-field region of the ^{1}H NMR spectra of the four decamers. In each case, 9−10 resonances can be observed, falling into two clusters corresponding to the imino protons of GC and AT(U) base pairs. The imino protons were assigned using NOESY in H_2O (not shown) which also provided the assignments of the Ade C2H. The N4H amino protons of the cytosines were assigned from NOEs between the GN1H of the base-paired G residue, and the H5 of the same cytosine residue. The hydrogen-bonded and non-hydrogen-bonded amino protons could also be discriminated using these NOEs. In none of the spectra was there any evidence for disproportionation into triple helices at any temperatures, nor in the presence of higher salt concentrations.

Despite the unfavorable sequences, the purine-rich strand gave good resolution in the base and H1′ regions, making the sequential assignment straightforward (Figure 4A). The pyrimidine resonances were much less well resolved, espe-

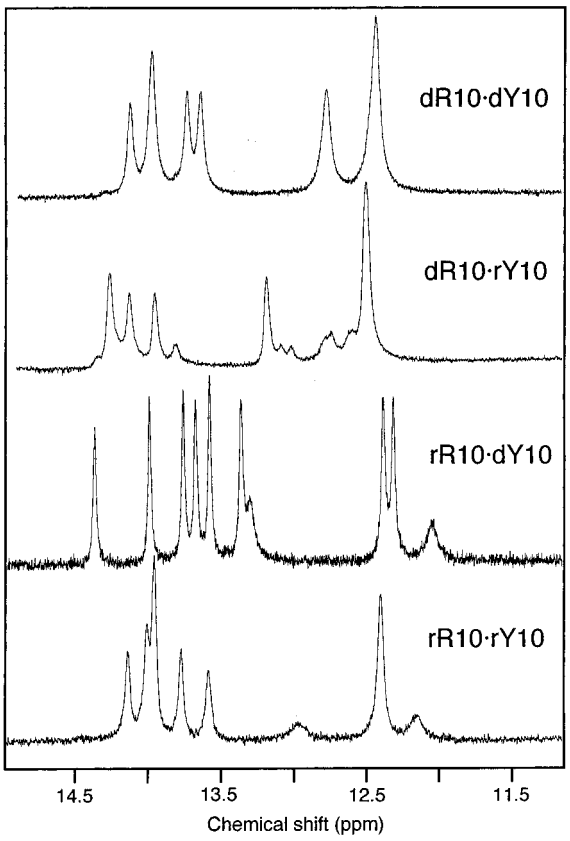

FIGURE 3: NMR spectra of the four duplexes in ^1H_2O. Spectra were recorded at 600 MHz, 10 °C, as described in Materials and Methods. Free induction decays were apodized using a 2 Hz line-broadening exponential. Low field region showing imino proton resonances.

cially those of thymidine H6, which can be attributed to the small ring current fields of the pyrimidines compared with the purines. Nevertheless, the sequential base−H1′ pathway could be traced. The remaining sugar protons were assigned using the NOEs from the assigned H1′ to H2′ and H2″, which were assigned stereospecifically because the NOE to H2″ is always larger than to H2′. The base and H2′/H2″ resonances were checked using the sequential NOEs between the base protons and the H2′, H2″ resonances. H3′ resonances were assigned using the sequential walk H8/H6(*i*)−H3′(*i*)−H8/6(*i*+1) in the same manner as for the base/H1′ resonances. The H3′ were confirmed using NOEs to the H2′ and from the cross-peaks H2′−H3′ in the DQF-COSY spectrum (see below). The H4′ were initially assigned using the NOEs from H1′ and confirmed using the H3′−H4′ cross-peaks in the DQF-COSY spectrum. With the exception of the unresolved H5′/H5″, all of the nonexchangeable protons were assigned.

r(GAAGAGAAGC)·d(GCTTCTCTTC). Figure 4B shows portions of a NOESY spectrum of the hybrid duplex r(GAAGAGAAGC)·d(GCTTCTCTTC). The H8−H1′ region of the RNA strand is well dispersed, making the sequential assignments via this pathway straightforward. The H2′ were assigned from the intense H1′−H2′ intraresidue cross-peaks. These assignments were confirmed from the sequential pathway H8(*i*)−H1′(*i*)−H2′(*i*)−H8(*i*+1) in NOESY spectra recorded with mixing times of 50 and 100 ms. H3′ resonances were assigned using both sequential and intraresidue NOEs to the assigned H8 and in some instances from DQF-COSY cross-peaks to the assigned H2′ resonances as previously described (Lane et al., 1993). The H4′ resonances were then found from correlations from the H1′ resonances in NOESY spectra and by noting the different cross-peak fine structure in the F_2 dimension for cross-peaks to H3′ and H4′, owing to their very different coupling patterns.

Although the H6−H1′ region of the NOESY spectra was relatively crowded, the combination the three sequential pathways as described for the DNA duplex (see above), the COSY connectivities for H1′ to both H2′ and H2″ as well as H2′−H3′ and H3′−H4′ made it possible to assign all of the nonexchangeable protons of the deoxypyrimidine nucleotides (except the H5′/H5″).

Also notable in Figure 4B is the presence of intense cross-peaks between the Ade C2H(*i*) and the H1′(*i*+1), both sequentially and across the duplex, compared with absence of the intraresidue AH2−H1′ (for which the distance is ca. 4.8 Å). This is consistent with substantial propeller twisting of the AU base pairs.

d(GAAGAGAAGC)·r(GCUUCUCUUC). Figure 4C shows a NOESY spectrum of the hybrid duplex d(GAAGAGAAGC)·r(GCUUCUCUUC). As for the DNA duplex, assignment of the purine strand was straightforward, and all but the H5′/H5″ resonances of the deoxyribose strand could be assigned using methods described for the DNA duplex above. The assignment of the ribose pyrimidine strand was more difficult because of the poorer dispersion, spectral overlap, and lack of correlation between H1′ and H2′ in the DQF-COSY experiment for all but the terminal residues (see below). However, by analyzing NOESY spectra recorded at different temperatures and mixing times, unambiguous assignments for all of the base and H1′ resonances were obtained. The H2′ resonances were assigned using the H1′−H2′ NOEs, which were checked against the base protons with the sequential pathways H6(*i*)−H1′(*i*)−H2′(*i*)−H6(*i*+1) (Figure 4C) as described above. Some H3′ resonances were assigned using H2′−H3′ correlations in the COSY experiment and H3′−H6 NOEs. Some H4′ were assigned from the H1′−H4′ NOE. However, the extensive overlap precluded complete assignment of the H3′ and H4′ resonances.

Notably strong cross-peaks were present for between Ade C2H(*i*) and H1′(*i*+1) on both strands. This is consistent with substantial propeller twisting of the AU base pairs, as observed with the other DNA·RNA hybrid (see above).

r(GAAGAGAAGC)·r(GCUUCUCUUC). Figure 4D shows a NOESY spectrum of the RNA duplex at 30 °C. The base and H1′ resonances were assigned using the NOE sequential pathway H8/H6(*i*)−H1′(*i*)−H8/H6(*i*+1), and H2′ from the H1′−H2′ intraresidue NOEs. The H2′ assignments were confirmed from the sequential H2′(*i*)−H8/H6(*i*+1) NOEs, which all appear intense. H4′ resonances were assigned from the H1′−H4′ NOE. The H3′ resonances were identified by their intra- and interresidue NOEs with the base protons, after eliminating the H2′ resonances. In some instances, H3′ and H4′ assignments could be confirmed from the DQF-COSY spectrum. However, some H4′ resonances could not be assigned, and some H3′ resonances in the pyrimidine strand remain ambiguous. Strong cross-peaks between AH2(*i*) and H1′(*i*+1) were present as observed in the two hybrid duplexes (see above).

The compositions and sequences of individual strands in the duplexes are identical. Hence, changes in chemical shifts between pure duplexes and the two hybrids should largely reflect differences in conformation. Figure 5 shows the

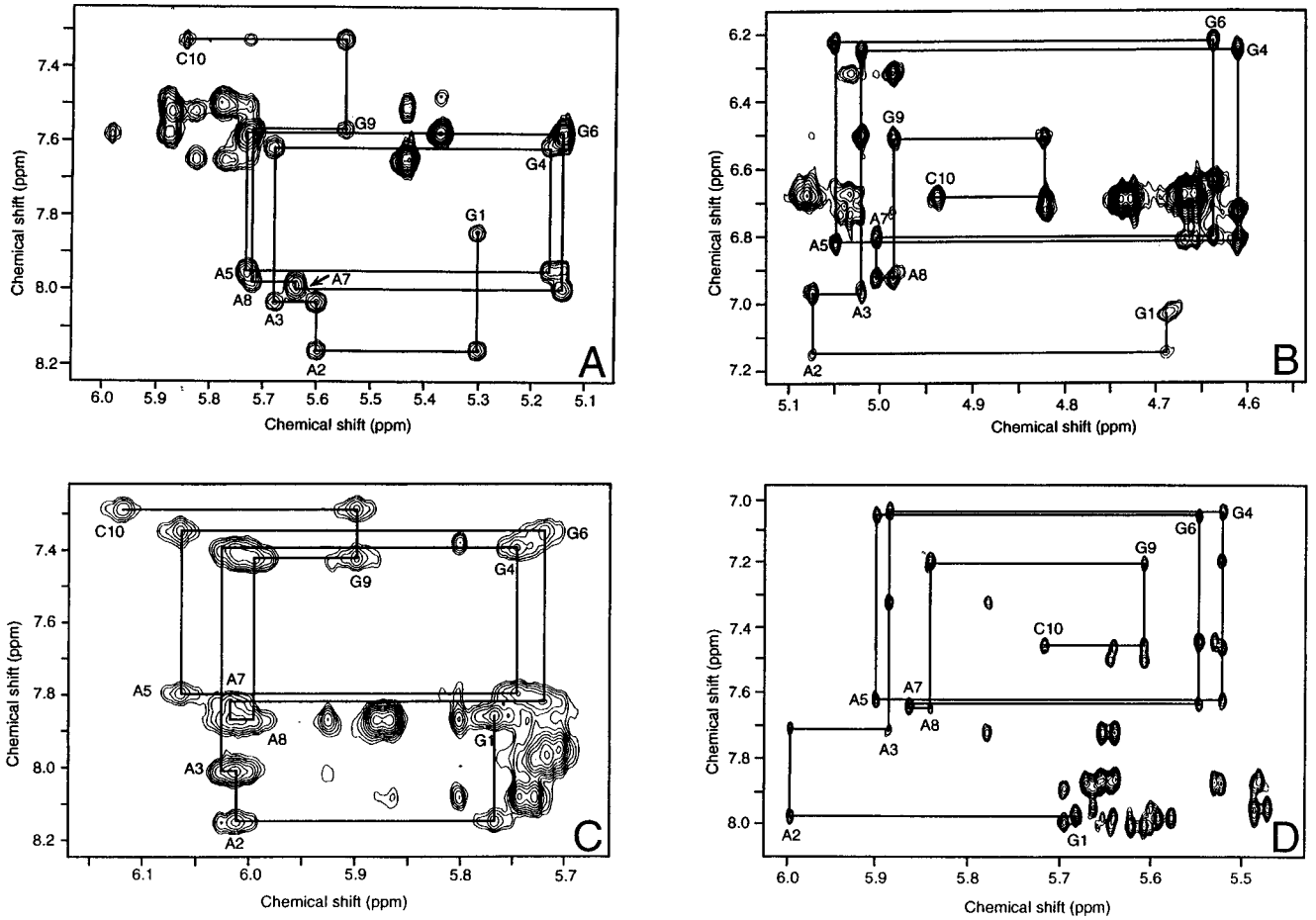

FIGURE 4: NOESY spectra of the duplexes in ^2H_2O. Spectra were recorded at 600 MHz, 30 °C, as described in Materials and Methods. Base proton−H1′ and C/U H6−H5 connectivities are shown. Spectra were zero-filled to 8192 × 2048 complex points, and apodized using a Gaussian function in both dimensions. (A) dR10·dY10. (B) rR10·dY10. (C) dR10·rY10. (D) rR10·rY10.

differences in proton chemical shifts between the hybrids and those of the DNA and RNA duplexes. The chemical shift differences were calculated as hybrid deoxyribose proton shifts minus DNA shifts and hybrid ribose proton shifts minus RNA shifts. We consider chemical shift changes of less than 0.05 ppm to be insignificant, as shown by the horizontal line at ±0.05 ppm. In the DNA strand of dR10·rY10, there are large positive shift differences for the H1′ protons and negative shift differences for the H8 and Ade C2H. In contrast, the deoxypyrimidines in rR10·dY10 in general show smaller shift differences, with the largest effects of H2′ (positive) and H2″ and H5 (negative). In the ribose purine strand, the shift differences are smaller on average than for the analogous comparison with the deoxypurines, and the signs of the changes are reversed. The smaller change in shifts for the ribose nucleotides is consistent with the conformation in the hybrids being similar to that in the pure RNA duplex. In contrast, the larger changes observed for the deoxynucleotides suggest that there is a substantial difference in conformation in the DNA strands between the pure DNA duplex and the DNA·RNA hybrids. Further, as the signs and absolute magnitudes of the shift differences differ for the two hybrids, it is plausible that the conformations are also somewhat different, which is supported by the electrophoretic and optical spectroscopy data (see above).

^{31}P NMR. ^{31}P chemical shifts have been reported to depend on backbone conformation (Gorenstein, 1992; Chou et al., 1992; Lane et al., 1992; Legault, & Pardi, 1994). We therefore recorded ^{31}P NMR spectra at 9.4 T as described in Materials and Methods. The chemical shift dispersions of the duplexes were in the order dR10·dY10 (0.45 ppm) < dR10·rY10 (0.60 ppm) < rR10·rY10(0.70 ppm) < rR10·dY10 (0.72 ppm) (spectra not shown). For comparison, the shift dispersion of an unrelated RNA duplex, r(CGCAAAU-UUGCG)$_2$ was 0.78 ppm under identical conditions (M. R. Conte, G. L. Conn, T. Brown, and A. N. Lane, unpublished data), and mixed-sequence DNA duplexes typically show a dispersion of shifts in the range 0.5−0.6 ppm (Gorenstein, 1992). Further, the center of the ^{31}P NMR spectra were essentially the same (approximately −17.3 ppm from methylene diphosphonate), suggesting similar backbone torsion angles on average. It appears that the range of phosphate shifts found in RNA is somewhat larger than in DNA duplexes. We also observed the relatively wide shift dispersion of 0.87 ppm in an octameric DNA·RNA hybrid of mixed sequence, which was shown to be globally closer to the A form than to the B form (Lane et al., 1993). The present results are consistent with the conformation of the rR10·dY10 hybrid duplex being closer to the A conformation adopted by RNA duplexes than the dR10·rY10 hybrid, which may have a more intermediate conformation at the level of

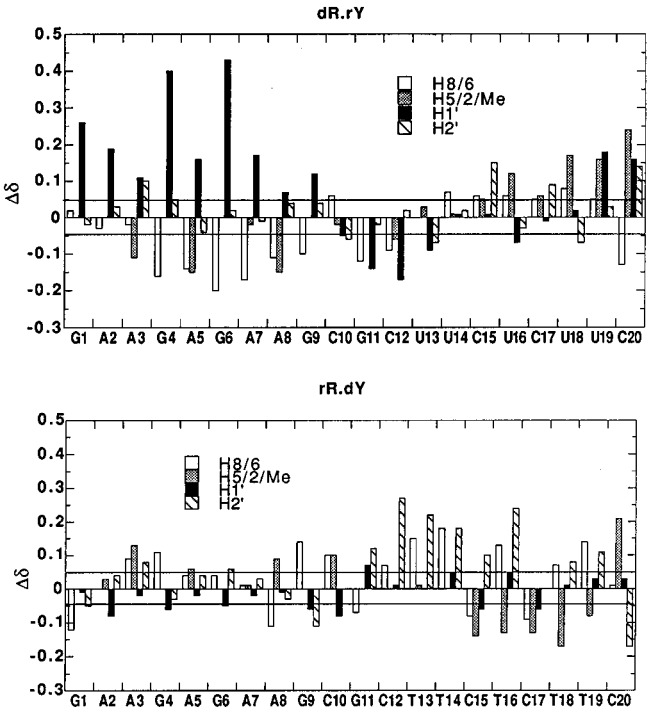

FIGURE 5: Chemical shift differences between the hybrid duplexes and the pure DNA and RNA duplexes. Chemical shift differences for selected protons were calculated from assignments made at 30 °C as described in the text. (Upper) Shift differences for the deoxyribose strands: *dR10*·rY10−*dR10*·dY10 and rR10·*dY10*−dR10·*dY10*. (Lower) Shift differences for the ribose strands: dR10·*rY10*−rR10·*rY10* and *rR10*·dY10−*rR10*·rY10.

the backbone torsion angles. This is consistent with the other spectroscopic data (see above).

Rotational Correlation Times. Rotational correlation times for the DNA and RNA duplexes were determined in two ways. First, measurements of the NOE build-up curves for the cytosine H6−H5 and uridine H6−H5 vectors were measured using 6−7 time points, and the effective correlation time was calculated from the cross-relaxation rate constant (Lane et al., 1986). The mean correlation time determined from the derived cross-relaxation rate constants was 3.2 ± 0.3 ns at 30 °C for the DNA duplex, which is typical of B-DNA in D_2O solution under these conditions (Birchall & Lane, 1990). Similarly, we obtained an effective rotational correlation time of 2.9 ± 0.3 ns at 30 °C for the RNA duplex.

Second, the spin−lattice and spin−spin relaxation rate constants of the phosphates were measured at 9.4 T and analyzed as described in Materials and Methods. Although the spectra were too crowded to assign by heteronuclear correlation experiments, the relaxation rate constants reflect mobility of the backbone. The relaxation data are summarized in Table 2. The correlation time for the DNA duplex was 3.6 ± 0.3 ns by ^{31}P relaxation, i.e., slightly larger than that obtained by ^{1}H−^{1}H cross-relaxation. The RNA duplex had an average correlation time of 3.2 ± 0.2 ns, again slightly larger than obtained from ^{1}H−^{1}H cross-relaxation (Table 2). This difference has been noted previously for DNA and may reflect different sensitivity of the two methods to internal motions (Lane, 1994). Although the correlation times for DNA and RNA are only slightly different compared with the experimental error, the consistent difference in two kinds of experiment is consistent with the RNA being more compact than the DNA as would be expected for A- and B-type duplexes, respectively. The correlation time determined by ^{31}P NMR for the rR10·dY10 hybrid duplex was 2.95 ± 0.24 ns, which is essentially identical to that determined for the RNA duplex and is consistent with a similar overall shape.

The effective chemical shift anisotropy was essentially identical for each duplex at ca. 150 ppm, which is comparable to values measured on other DNA duplexes in DNA in general (Forster & Lane, 1990), and demonstrates that ^{31}P line widths are dominated by CSA at magnetic field strengths of 9.4 T or higher.

Sugar Conformations of the Riboses. With the exception of terminal residues, there were no observable correlations between H1′ and H2′ of the riboses in DQF-COSY spectra recorded with acquisition times up to 0.09 s in t_1. Strong cross-peaks were observed, however, for H3′−H4′. The ribose H1′ that were resolved in the 1D spectra appeared as singlets, with line widths of <3 Hz. This is also evident in the NOESY spectra (Figure 4B−D) where the ribose H1′ resonances are narrow along F_2, compared with the H1′ resonance of the deoxyriboses, which appear as triplets. This indicates $^3J_{1'2'}$ of <2−3 Hz, which places the ribose conformations in the N domain ($-32 < P < 32$). This indicates that the riboses in all three RNA-containing duplexes have sugar conformations in the "N" domain. Even for terminal residues, the H1′−H2′ cross-peaks in the DQF-COSY spectra were very weak, also indicating that these residues, while having possibly greater conformational freedom than internal residues, are also largely in the "N" domain.

Sugar Conformations of the Deoxyriboses. Sums of coupling constants derived from cross-sections of DQF-COSY and NOESY, and where possible 1D spectra, are given in Table 3. In addition, the distance H1′−H4′ was estimated from NOESY spectra as described in Materials and Methods. This distance is at a minimum for $P_s = 90°$ (O4′-endo) and increases sharply in the ranges $100 < P_s < 162$ and $90 > P_s > 18$ (van de Ven & Hilbers, 1988). It is therefore a useful adjunct to coupling constants for differentiating between unique conformations with $P \approx 90°$ (Salazar et al., 1993) and mixtures of N and S conformations (Conte et al., 1996).

In the pure DNA duplex, the intensities of the DQF-COSY H1′−H2′ cross-peaks are much greater than the H1′−H2″ cross-peaks, and similarly for H2′−H3′ versus H2″−H3′. The cross-peaks also show considerable antiphase fine structure, viz., ++−− for H2′−H1′ and +−+− for H2″−H1′ (Figure 6). Indeed, this structure is evident for essentially all of the cross-peaks (C20 is an exception where H2′ and H2″ are nearly isochronous) indicating significantly different values of $^3J_{1'2'}$ and $^3J_{1'2''}$. Further, $\sum_{1'}$ (= $^3J_{1'2'}$ + $^3J_{1'2''}$) is >14.5 Hz for all residues except the terminal nucleotides, showing that the nucleotides are predominantly in the "S" domain (van Wijk et al., 1992). This is supported by the relatively small values of $\sum_{3'}$ and the value of $r_{1'4'}$ (>3 Å). Because extensive data for the sugars of the purine strand are available, a detailed examination of the sugar conformation can be made.

The sums of the coupling constants and $r_{1'4'}$ cannot be rationalized as a single, unique conformation. We have therefore used a two-state N/S equilibrium model to analyze these data. Conformational mixtures as a function of f_s and

Table 3: Sugar Conformations of Deoxyriboses[a]

nucleotide	$\Sigma_{1'}$ (Hz)	$\Sigma_{2'}$ (Hz)	$\Sigma_{2''}$ (Hz)	$\Sigma_{3'}$ (Hz)	$r_{1'4'}$ (Å)	P_s (deg)	f_s
dR10·dY10							
G1	15.1	30.4	21.2	nd	3.0	140	0.92
	$^3J_{1'2'} = 9.5$, $^3J_{1'2''} = 5.6$						
A2	15.3	30	21	nd	3.05	167	0.92
	$^3J_{1'2'} = 9.8$, $^3J_{1'2''} = 5.5$						
A3	15.0	nd	nd	nd	3.0	148	0.91
	$^3J_{1'2'} = 9.5$, $^3J_{1'2''} = 5.5$						
G4	14.6	30	21	nd	2.9	126	0.88
A5	nd	30	21	nd	3.1	153	0.88
G6	14.4	nd	nd	12.9	2.9	126	0.85
A7	15.0	nd	nd	14.4	3.0	135	0.91
	$^3J_{1'2'} = 8.8$, $^3J_{1'2''} = 6.2$						
A8	15.3	nd	nd	nd	3.0	S	0.93
G9	14.4	30.3	23.2	15.9	3.1	135	0.84
	$^3J_{1'2'} = 8.0$, $^3J_{1'2''} = 6.4$						
C10	14	29.2	nd	nd	3.0	135	0.78
mean	14.9	30.1	21.5	14.4	3.0	141	0.89
sd	±0.4	±0.2	±0.9	±1.2	±0.07	±13	±0.03
G11	14.2	29.8	nd	16.2	3.2	144	0.7
C12	nd	nd	nd	16	2.85	≈120	≈0.7
T13	15.0	nd	nd	16.2	nd	S	0.9
	$^3J_{1'2'} = 9.2$, $^3J_{1'2''} = 5.8$						
T14	15.2	31	nd	nd	2.85	126	0.92
C15	14.1	nd	nd	15.5	nd	≈120	0.7
T16	nd	30.5	nd	12	nd	≈130	≈0.9
C17	14.9	nd	nd	16	3.0	135	0.86
T18	14.7	nd	nd	nd	2.9	S	0.83
T19	14.6	nd	24	nd	3.0	108	0.82
C20	13.8	nd	nd	16.2	3.0	S	0.68
mean	14.7	30.4		15.3	2.97	125	0.83
sd	±0.4	±0.5		±1.5	±0.12	±12	±0.07
rR10·dY10							
G11	13.2	30	25	nd	nd	103	0.67
C12	13.3	28	nd	15	3.0	125	0.7
T13	13.1	29	26	nd	2.8	140	0.7
T14	13.3	28	23	12	2.8	150	0.66
C15	12.7	28	nd	14	2.9	148	0.58
T16	13.2	28	nd	12	2.8	162	0.66
C17	12.3	27	26	14	2.8	152	0.55
T18	13.0	29	nd	nd	2.8	110	0.67
T19	14.2	30	27	12	2.9	138	0.82
C20	13.9	29	25	15	2.9	128	0.75
mean	13.1	28.6	25.3	13.2	2.85	136	0.67
sd	±0.5	±1	±1.2	±1.2	±0.07	±20	±0.07
dR10·rY10							
G1	14.2	28	23	14	2.85	130	0.78
A2	nd	nd	nd	14	nd	S	nd
A3	14.5	nd	24	16.7	2.8	108	0.87
G4	14.5	nd	nd	12	2.95	135	0.87
A5	14.0	31	23	nd	3.0	135	0.78
G6	14.5	30	23	15	3.0	130	0.86
A7	14.1	nd	nd	11	3.1	158	0.78
A8	13.8	31	25	nd	2.95	140	0.75
G9	13.5	30	25	nd	3.0	135	0.69
C10	14.0	30	26	nd	2.9	131	0.78
mean	14.1	30	23.8	13.8	2.95	134	0.79
sd	±0.4	±1.1	±0.9	±1.9	±0.08	±13	±0.06

[a] $\Sigma_{3'}$ includes $^3J_{H3'-P}$ (4−6 Hz). Values of P_s and f_s calculated as described in the text. The standard deviations were estimated as ±0.5 Hz for $\Sigma_{1'}$, ±1 Hz for $\Sigma_{2'}$, and ±2 Hz for $\Sigma_{2'}$ and $\Sigma_{3'}$. The lower limit to $r_{1'4'}$ was set to 0.1 Å below the extrapolated value at zero mixing time, and the upper limit to this value +0.5 Å. Errors on P_s and f_s are estimated at ±20° and ±0.1, respectively. nd, not determined.

P_s were systematically generated, and the calculated coupling constants and distances were compared with the experimental data using the program pfit (Conte et al., 1996). The resulting values for f_s and P_s are given in Table 3. Not surprisingly, the values of f_s are relatively high (>0.85), and P_s is in the "S" range (ca. 130−160°), which is typical of B-DNA. Fewer data were obtained for the pyrimidine strand, though the combination of the values of $\Sigma_{1'}$ and $r_{1'4'}$ and the observation that $^3J_{1'2'} > {}^3J_{1'2''}$ (see above) suggest that the pyrimidines have on average similar sugar conformations as the purines. There is no significant difference in $\Sigma_{1'}$ between the two strands, on average, though there may be a tendency for the pyrimidines to adopt a lower pseudorotation phase angle (Table 3).

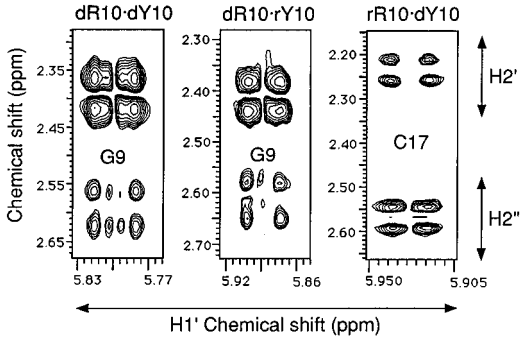

FIGURE 6: Comparison of DQF-COSY cross-peaks in the DNA and DNA·RNA hybrid duplexes for the H1′ to H2′/H2″ regions. Spectra were recorded at 500 MHz and 30 °C as described in Materials and Methods. Spectra were transformed from matrices of 8192 × 2048 complex points, with a shifted Gaussain function to provide apodization and mild resolution enhancement. The digital resolution was 1.22 Hz/point along F_2 and 4.88 Hz/point along F_1. Left, G9 of dR10·dY10; middle, G9 of dR10·rY10; right, C17 of rR10·dY10

In contrast to the DNA duplex, the intensities of the H1′−H2′ and H1′−H2″ cross-peaks are more similar in the hybrid duplex rR10·dY10, and there is little fine structure (Figure 6). Also, the H2″−H3′ cross-peaks are relatively more intense (not shown). Further, as Table 3 shows, the values of $\sum_{1'}$ are significantly smaller, in the range 12.3−14.2 Hz (mean = 13.3 ± 0.5 Hz). This indicates a lower conformational purity and/or rather smaller values of P_s. In addition, there is much less fine structure in the cross-peaks, which indicates that $^3J_{1'2'} \approx {}^3J_{1'2''}$. This is consistent with a unique sugar conformation only if $P_s \approx 200-220°$. However, neither the values of $\sum_{2'}$ and $\sum_{2''}$ nor $r_{1'4'}$ are consistent with such a conformation. Further, the $r_{1'4'}$ distances are significantly smaller (ca. 2.8−2.9 Å on average) than in the DNA duplex. This requires a smaller value of P_s for than in the DNA duplex (van Wijk et al., 1992). We note, for a single conformation, that a value of $P_s \approx 108°$ is required to account of the low value of $r_{1'4'}$, but this then predicts that $\sum_{1'} \approx 16$ Hz, which is much larger than is observed (Table 3). We conclude that a unique conformation is not consistent with the data. The conformations given in Table 3 were calculated assuming an N/S equilibrium, as described for the DNA duplex.

The hybrid duplex dR10·rY10 appears more similar to the DNA duplex, with the cross-peak intensities H1′−H2′ ≫ H1′−H2″ (Figure 6) and H2′−H3′ > H2″−H3′. However, the fine structures are significantly different. Thus, whereas the H1′−H2′ cross-peak of G9 in the hybrid shows a simple +− fine structure, the fine structure is ++−− in the DNA duplex. Similarly, in the hybrid, the H1′−H2″ fine structure for G9 is +−, whereas in the DNA duplex, it is +−+−. The values of $\sum_{1'}$ (Table 3) are in the range 13.4−14.5 Hz (mean 14 ± 0.35 Hz), which is smaller than for the purine strand in the pure DNA duplex but larger than for the pyrimidines in rR10·dY10. Further, values of $r_{1'4'}$ of 2.9−3 Å on average, and $\sum_{3'} < 16$ Hz (including the $^3J_{H3'P}$ of ca. 4−6 Hz) rule out major conformations with $P_s < 108°$ (van Wijk et al., 1992). The data in Table 3 were analyzed using the N/S two-state equilibrium, from which typical values for P_s of ca. 135°, and f_s values in the range 0.7−0.9 were obtained.

The data given in Table 3 show that the sugar conformations in the DNA duplex are typical of B-DNA, with the possibility that P_s in the pyrimidine strand on average is smaller than P_s in the purine strand. It is clear that the DNA strands in the DNA·RNA hybrids have different conformations from their counterparts in the pure DNA duplex, with possibly a lower value of P_s, and a significantly smaller value of f_s, which indicates a higher degree of flexibility. This is in agreement with our previous findings (Lane et al., 1993) and a recent detailed study of a mixed-sequence DNA·RNA hybrid (Gonzalez et al., 1994, 1995). It is also evident that the two DNA·RNA hybrids are not equivalent, such that the deoxyriboses in rR10·dY10 are more flexible on average than those in dR10·rY10.

Table 4: Glycosidic Torsion Angles[a]

base	*dR10*·dY10 (−χ/deg)	*dR10*·rY10 (−χ/deg)	*rR10*·dY10 (−χ/deg)	base	rR10·*dY10* (−χ/deg)	dR10·*dY10* (−χ/deg)
G1	125	nd	170	G11	145	anti[b]
A2	115	125	155	C12	107	120
A3	115	125	170	T13	125	120
G4	125	130	130	T14	130	120
A5	nd	125	150	C15	108	115
G6	125	125	150	T16	120	anti
A7	110	125	170	C17	130	115
A8	110	125	155	T18	115	120
G9	nd	128	150	T19	150	anti
C10	130	135	170	C20	115	130

[a] Torsion angles were determined by nonlinear regression to intranucleotide NOE time courses as described in Materials and Methods. Estimated errors are ±5° for deoxynucleotide and ±10° for ribonucleotides. Data refer to the italicized strand. [b] Based on H1′−H8 intranucleotide NOE intensity.

Glycosidic Torsion Angles. Intranucleotide NOE intensities were typical of the *anti* conformation about the glycosidic bond. For the deoxynucleotides, the H8/H6−H2′ NOEs were much larger than either H8/H6−H1′ or H8/H6−H3′, and consistent with χ in the range −90° to −120° in the DNA duplex, and −100° to −130° in the hybrid duplexes. For the ribonucleotides, the H8/H6−H1′ and H2′ NOEs were very weak compared with the H8/H6−H3′ NOE, as expected for a C3′-endo pucker and $\chi \approx -160°$. Where sufficient cross-peaks were resolved, the glycosidic torsion angles were analyzed in greater detail with NUCFIT (Lane, 1990) using the time courses of the NOEs from H8/H6 to H1′, H2′(H2″), and H3′. The deoxynucleotides were analyzed as a conformational blend of S and N states, with sugar conformations and the fraction of the S state sampled at values around those determined from the coupling constants (see above). The ribonucleotides were assumed to consist of a single conformation with $P \approx 9°$. The precise value of P within a conformational range (i.e., S or N) has little influence on the determination of the glycosidic torsion angle (Lane, 1990). The values of χ determined in this way are given in Table 4. Because there is a high ratio of data to parameters in these calculations, the glycosidic torsion angles are well determined. In general it can be seen that the torsion angles are highest for the deoxynucleotides in the DNA duplex, followed by the deoxynucleotides in the two hybrids, and are lowest in the ribonucleotides. Indeed, the glycosidic torsion angles of the ribonucleotides are similar whether they are in a pure RNA duplex or DNA·RNA hybrid, whereas the angles are significantly different between the pure DNA duplex and the two hybrid duplexes. This also suggests that much of the conformational differences between the hybrid duplexes arises from the nucleotide conformations in the DNA strands. This is consistent with the observed changes

Table 5: Relative H2′(*i*)−H8/H6(*i*+1) Distances in the RNA Strands[a]

rR10·rY10		rR10·*rY10*	
G1−A2	2.8	G11−C12	2.9
A2−A3	3.1	C12−U13	2.7
A3−G4	2.8	U13−U14	2.5
G4−A5	2.7	U14−C15	(2.5)[b]
A5−G6	3.0	C15−U16	2.6
G6−A7	2.7	U16−C17	(2.6)[b]
A7−A8	2.8	C17−U18	2.6
A8−G9	2.9	U18−U19	2.4
G9−C10	2.7	U19−C20	2.7
mean ± sd	2.8 ± 0.1		2.6 ± 0.1
rR10·dY10		dR10·*rY10*	
G1−A2	3.0	G11−C12	2.3
A2−A3	3.0	C12−U13	nd
A3−G4	2.7	U13−U14	2.3
G4−A5	2.8	U14−C15	nd
A5−G6	2.8	C15−U16	nd
G6−A7	2.7	U16−C17	nd
A7−A8	2.7	C17−U18	nd
A8−G9	2.8	U18−C19	2.2
G9−C10	2.6	U19−C20	2.2
mean ± sd	2.8 ± 0.1		

[a] Cross-peak volumes were measured using Felix 95.0 and normalized to the average of the nonterminal Cyt H6−H5 or UH6−H5 cross-peak volumes. The distances were calculated as $r = 2.45V_n^{-1/6}$, where V_n is the normalized volume, and extrapolating back to zero mixing time. Data refer to the italicized strand. nd, not determined. [b] Overlapping peaks.

in chemical shifts for the DNA protons between the hybrid duplexes and the DNA duplex (see above).

Global Conformations. The CD spectra indicate that the DNA duplex is B form and the RNA duplex is A form. This was confirmed by the NMR results, which showed nucleotide conformations typical for the B and A forms, respectively. In addition, the internucleotide NOE intensities were also consistent with B and A. The CD spectra of the two hybrids indicate the presence of conformations at the level of base-stacking interactions of conformations intermediate between the A and B structures. The electrophoretic mobilities, apparent correlation times, and ^{31}P NMR shift dispersions are consistent with a ranking of conformations from dR10·dY10 (most B-like) through dR10·rY10, rR10·dY10 to rR10·rY10 (most A-like).

The H2′(*i*)−H8/6(*i*+1) distance is short (<2.5 Å) in the A conformation and long (>3.5 Å) in the B-conformation, and therefore the corresponding NOE intensities provide a sensitive indicator of the structure of the ribose strands. We have measured the intensities of the H2′(*i*)−H8/H6(*i*+1) cross-peaks in the RNA strands as a function of mixing time. The distances have been calculated assuming a distance of 2.45 Å for the Cyt H6−H5 vector (Table 5). In the RNA·RNA duplex, the normalized cross-peak volumes for the pyrimidines are near unity for all mixing times (50−400 ms), which implies that the distance is about 2.5 Å. In contrast, the normalized volumes for the purines approach unity at long mixing times (250−400 ms) but decrease to ca. 0.2−0.3 at the shortest mixing time. This indicates that the H2′(*i*)−H8(*i*+1) distance in the purine strand is longer than that of the reference vector (2.45 Å) and is closer to 3 Å. We note that this is not predicted by the standard A structure ($r \approx 1.6$ Å) or even one that has been energy minimized ($r \approx$ 2.3 Å). This indicates some structural asymmetry between the two strands of this particular RNA duplex.

A similar pattern was observed in the two hybrids. The normalized H2′(*i*)−H8/H6(*i*+1) cross-peak intensity in rR10·dY10 decreased with decreasing mixing time (250 to 50 ms), reaching a limiting value of ca. 0.3 at short mixing times. This is equivalent to a distance of around 3−3.2 Å. In contrast, the normalized intensities for the pyrimidine strand in dR10·rY10 increased slightly with decreasing mixing time, reaching a limiting value of 1−1.5 at short mixing time, and consistent with a distance of 2.3−2.4 Å. Hence, the sequential H2′(*i*)−H8(*i*+1) and H2′(*i*)−6(*i*+1) are preserved in the RNA strands of the two hybrids. Overall, these distances indicate that the RNA strands are globally closer to the A conformation than to the B conformation, in the hybrids as well as in the RNA duplex.

In contrast, the H2′(*i*)−H8/H6(*i*+1) intensities in the DNA strands were weak compared with the H2″−H8/H6 intensities. In the pure DNA duplex, the observed intensity largely reflects spin diffusion via H2″. The observed H2″−H8/H6 distances were ca. 3 Å (not shown), which is longer than expected for standard B-DNA but is typical of DNA in solution.

These data, and the analysis of the conformations of the deoxy strands, clearly show significant conformational differences between the two DNA·RNA hybrids, and of course compared with the pure DNA and RNA duplexes. Further, the conformations of the RNA strands in the hybrids are similar to their conformations in the RNA duplex, whereas there are differences between the conformations of the DNA strands in the hybrids and the DNA duplex.

DISCUSSION

We have confirmed the extensive thermodynamic behavior of this class of DNA·RNA hybrids and also the global conformational features (Ratmeyer et al., 1994; Hung et al., 1994; Lesnik & Freier, 1995; Sugimoto et al., 1995; Wang & Kool, 1995). The present data show that the DNA duplex, as expected, is in the B family of conformations, and the RNA duplex is in the A conformation. Clearly the DNA·RNA hybrids, while overall more A-like than B-like, are in an intermediate state. Moreover, this intermediate state is clearly different for the two hybrids, both globally and at the nucleotide level in the DNA strands. According to the spin−spin coupling data, this is manifested in particular in the degree of flexibility of the DNA strands, which is greater in the hybrids than in the DNA duplex, and on average the deoxypyrimidine nucleotides are more flexible than the deoxypurines. Also, the changes in ^{1}H chemical shifts are much larger for the DNA strands than for the RNA strands, but the pattern of shifts for the two nucleotides is quite different. This indicates that the major conformational rearrangements between the pure duplexes and the hybrids occur in the DNA strands, and that the conformational changes are not the same in the two hybrid duplexes. The differences at the local level translate into differences in base stacking, as observed in the CD spectra and sequential NOE intensities, backbone conformation as seen in the ^{31}P NMR spectra, and overall in the differences in hydrodynamic and electrophoretic behavior. The differences in base-stacking may account, at least in part, for the observed differences in thermodynamic stabilities. It is clear that there is more

flexibility in the DNA·RNA hybrids than in either of the two pure duplexes, and presumably this in part affects the differences in stability through the configurational entropy changes between the strand and duplex states. We have detected experimentally flexibility at the nucleotide level. How widespread this is and the contributions to the different thermodynamic stabilities must await full three-dimensional structure determinations. These calculations are in progress. However, because of the effects of conformational averaging, rather more detailed structures calculations have to be carried out for these duplexes, such as the use of time averaged distance restraints as recently applied to a DNA·RNA hybrid (Gonzalez et al., 1995), or based on local conformational averaging, where appropriate ensembles of conformations are calculated that account for the experimental NOEs and coupling constants.

Based on our results and information in the literature regarding the solution conformation of DNA·RNA hybrids (Fedoroff et al., 1993; Lane et al., 1993; Gonzalez et al., 1994, 1995), it is likely that the backbone conformation and/or minor groove widths of the two classes of hybrid also differ significantly. If the activity of RNAseH is sensitive to minor groove width and backbone conformation, then we would expect that the enzyme would cleave rR10·dY10 at a different rate to dR10·rY10. It has been suggested that RNAse H activity increases the *in vivo* efficiency of antisense technology (by destroying the target mRNA and releasing the DNA) (Walder & Walder, 1988). This could provide an additional facet to the design of optimum antisense DNA molecules. It would therefore be of considerable practical interest to determine the relative rates of cleavage of mixed-sequence DNA·RNA hybrids versus the all-pyrimidine and all purine RNA strands.

ACKNOWLEDGMENT

We thank Dr. S. Martin for assistance with the circular dichroism. We are grateful to Dr. M. R. Conte for critical appraisal of the manuscript.

SUPPORTING INFORMATION AVAILABLE

Four tables and three figures of NMR assignments, UV melting curves, additional NOESY, and DQF-COSY spectra (14 pages). Ordering information is given on any current masthead page.

REFERENCES

Adams, R. L. P., Knowler, J. T., & Leader, D. P. (1986) *The Biochemistry of the Nucleic Acids*, 10th ed., Chapter 6, Chapman and Hall, London.
Bax, A., & Davis, D. G. (1985) *J. Magn. Reson. 65*, 355−360.
Birchall, A. J., & Lane, A. N. (1990) *Eur. Biophys. J. 19*, 73−78.
Breslauer, K. J., Frank, R., Blocker, H., & Marky, L. A. (1986) *Proc. Natl. Acad. Sci. U.S.A. 83*, 3746−3750.
Brown, T., & Brown, D. J. S. (1991) in *Oligonucleotides and Analogues, a Practical Approach* (Eckstein, F., Ed.) pp 1−23, IRL Press, Oxford.
Brown, T., & Brown, D. J. S. (1992) *Methods Enzymol. 211*, 20−35.
Chou, S.-H., Cheng, J.-W., & Reid, B. R. (1992) *J. Mol. Biol. 228*, 138−155.
Conte, M. R., Bauer, C. J., & Lane, A. N. (1996) *J. Biomol. NMR 7*, 190−206.
Ebel, S., Brown, T., & Lane, A. N. (1994) *Eur. J. Biochem. 220*, 703−715.
Fasman, G. D., Ed. (1975) *Handbook of Biochemistry and Molecular Biology. Nucleic Acids*, Vol. I, 3rd ed., p 589, CRC Press, Boca Raton, FL.
Fedoroff, O. Y., Salazar, M., & Reid, B. R. (1993) *J. Mol. Biol. 233*, 509−523.
Feigon, J., Koshlap, K. M., & Smith, F. W. (1995) *Methods Enzymol. 261*, 225−255.
Freier, S. M., Kierzek, R., Jaeger, J. A., Sugimoto, N., Caruthers, M. H., Neilson, T., & Turner, D. H. (1986) *Proc. Natl. Acad. Sci. U.S.A. 83*, 9373−9377.
Forster, M. J., & Lane, A. N. (1990) *Eur. Biophys. J. 18*, 347−355.
Gonzalez, C., Stec, W., Kobylanska, A., Hogrefe, R. I., Reynolds, M., & James, T. L. (1994) *Biochemistry 33*, 11062−11072.
Gonzalez, C., Stec, W., Reynolds, M., & James, T. L. (1995) *Biochemistry 34*, 4969−4982.
Gorenstein, D. G. (1992) *Methods Enzymol. 211*, 254−286.
Hall, K. B., & McLaughlin, L. W. (1991) *Biochemistry 30*, 10606−10613.
Hansen, U. M., & McClure, W. R. (1980) *J. Biol. Chem. 255*, 9564−9570.
Hung, S.-H., Yu, Q., Gray, D. M., & Ratliff, R. L. (1994) *Nucleic Acids Res. 22*, 4326−4334.
Ivanov, V. I., Minchenkova, L. E., Minyat, E. E., Frank-Kamenetskii, M. D., & Schyolkina, A. K. (1974) *J. Mol. Biol. 87*, 817−833.
Lane, A. N. (1990) *Biochim. Biophys. Acta 1049*, 189−204.
Lane, A. N. (1994) *Prog. NMR Spectrosc. 25*, 481−505.
Lane, A. N., & Fulcher, T. (1995) *J. Magn. Reson. B 106*, 34−42.
Lane, A. N., Lefèvre, J.-F., & Jardetzky, O. (1986) *J. Magn. Reson. 66*, 201−208.
Lane, A. N., Jenkins, T. C., Brown, D., & Brown, T. (1991) *Biochem. J. 279*, 269−281.
Lane, A. N., Martin, S. R., Ebel, S., & Brown, T. (1992) *Biochemistry 31*, 12087−12095.
Lane, A. N., Ebel, S., & Brown, T. (1993) *Eur. J. Biochem. 215*, 297−306.
Legault, P., & Pardi, A. (1994) *J. Magn. Reson. 103B*, 82−86.
Lesnik, E. A., & Freier, S. M. (1995) *Biochemistry 34*, 10807−10815.
Oda, Y., Iwai, S., Ohtsuka, E., Ishikawa, M., Ikehara, M., & Nakamura, H. (1993) *Nucleic Acids Res. 21*, 4690−4695.
Pilch, D. S., Levenson, C., & Shafer, R. H. (1990) *Proc. Natl. Acad. Sci. U.S.A. 87*, 1942−1946.
Piotto, M., Saudek, V., & Sklenar, V. (1992) *J. Biomol. Struct. Dyn. 2*, 661−665.
Ratmeyer, L., Vinayak, R., Zhong, Y. Y., Zon, G., & Wilson, W. D. (1994) *Biochemistry 33*, 5298−5304.
Salazar, M., Champoux, J. J., & Reid, B. R. (1993a) *Biochemistry 32*, 739−744.
Salazar, M., Fedoroff, O. Y., Miller, J. M., Ribeiro, N. S., & Reid, B. R. (1993b) *Biochemistry 32*, 4207−4215.
States, D. J., Haberkorn, R. A., & Ruben, D. J. (1982) *J. Magn. Reson. 48*, 286−292.
Stein, C. A., & Cheng, Y.-C. (1993) *Science 261*, 1004−1012.
Stein, H., & Hausen, P. (1969) *Science 166*, 393−395.
Sugimoto, N., Nakano, S.-i., Katoh, M., Matsamura, A., Nakamuta, H., Ohmichi, T., Yoneyama, M., & Sasaki, M. (1995) *Biochemistry 34*, 11211−11216.
van de Ven, F. J. M., & Hilbers, C. W. (1988) *Eur. J. Biochem. 178*, 1−38.
Varmus, H. (1988) *Science 240*, 1427−1435.
Walder, R. Y., & Walder, J. A. (1988) *Proc. Natl. Acad. Sci. U.S.A. 85*, 5011−5015.
Wang, S. H., & Kool, E. T. (1995) *Biochemistry 34*, 4125−4132.
van Wijk, J., Huckriede, B. D., Ippel, J. H., & Altona, C. (1992) *Methods Enzymol. 211*, 286−306.
Williamson, J. R., & Boxer, S. G. (1989) *Biochemistry 28*, 2819−2831.
Wincott, F., DiRenzo, A., Shaffer, C., Grimm, S., Tracz, D., Workman, C., Sweedler, D., Gonzalez, C., Scaringe, S., & Usman, N. (1995) *Nucleic Acids Res. 23*, 2677−2684.

BI960948Z